

Stability Satisfied Numerical Approximates to the Non-analytical Solutions of the Cubic Schrödinger Equation

Alper Korkmaz*

Çankırı Karatekin University, Department of Mathematics, 18200, Çankırı, Turkey.

November 22, 2016

Abstract

The time dependent complex Schrödinger equation with cubic nonlinearity is solved by constructing differential quadrature algorithm based on sinc functions. Reduction to a coupled system of real equations enables to approach the space derivative terms by the proposed method. The resulted ordinary differential equation system is integrated with respect to the time variable by using a bunch explicit methods of lower and higher orders. Some initial boundary value problems containing some analytical and non-analytical initial data are solved for experimental illustrations. The computational errors between the analytical and numerical solutions are measured by the discrete maximum error norm in case the analytical solution exists. The two conserved quantities are calculated by using the numerical results in all cases. The matrix stability analysis is implemented to control the time step size.

Keywords: Cubic Schrödinger equation; differential quadrature method; stability; soliton.

1 Introduction

Consider the cubic nonlinear Schrödinger (NLS) equation of the canonical form [1]

$$i \frac{\partial u(x, t)}{\partial t} + \frac{\partial^2 u(x, t)}{\partial x^2} + \kappa |u(x, t)|^2 u(x, t) = 0, \quad -\infty < x < \infty, \quad t > 0 \quad (1)$$

*alperkorkmaz7@gmail.com

where $u = u(x, t) \in \mathbb{C}$. This equation is a standard dimensionless form of the Talanov's model [2] describing stationary light beam of plane form in a medium with nonlinear refractive index and quasimonochromatic one-dimensional wave in a dispersive and inertialess nonlinear medium [1, 3, 4]. The solutions are named as self-focusing or defocussing according to the sign of the coefficient of the nonlinear term κ in the propagating of electromagnetic waves [5]. The NLS equation disallows steady soliton solutions traveling with a constant speed [6]. Alternatively, it has envelop soliton solutions containing both exponential and sech functions traveling with different speeds [6]. Zakharov and Shabat [1] applied the inverse scattering method successfully to develop exact solutions of some dynamic problems to the cubic NLS equation (1). Debnath [6] summarizes the findings of Zakharov and Shabat [1] as

- An initial envelope pulse breaks into permanent, propagating, shorter scaled solitons the number of which depends on the initial data and an oscillatory tail,
- Separates after interaction without changes except possible position or phase changes,
- The oscillatory tail whose nature is defined in the initial data disperses linearly with a decaying amplitude as $t \rightarrow \infty$,

when the initial data converge zero as $|x| \rightarrow \infty$.

An envelop-type soliton also behaves like a particle familiar to the KdV soliton [7]. The amplitude of the envelop of the one soliton solution of the cubic NLS equation (1) is of permanent form describing a physical wave which is in a good agreement with Hammack's unpublished experiment data [8].

Recurrence is also significant for the solutions of the NLS equation in bounded or periodic domains [6]. The relation between the recurrence, dimensionality, and the stability in the Lagrange sense of solutions of the cubic NLS equation is investigated in details by Thyagaraja [9].

The equation can be a model for the vortex line in an imperfect Bose gas with weak pair repulsions between atoms [10]. In addition to be an approximation for beams of the modulated form in nonlinear optics, the NLS is a significant equation for the time dependent dispersive waves [11].

Tsuzuki [12] examines deeply the nonlinear solitary and periodic waves for a particular type of the NLS equation. Some conservations laws describing the quantities density, current and energy are derived in integral form for that particular type. The collision of two positive solitaries with different heights traveling to the right in the horizontal axis is also discussed. In the last part of this study, the wave generation in terms of the decay of an arbitrary initial disturbance into solitary waves is investigated, too.

Some of the exact solutions covering interaction of solitary wave packets and n -soliton solutions of the cubic NLS equation are derived by transforming it to a problem of inverse scattering. Some conservation laws describing various quantities for the NLS equation (1) are also defined in [1]. The direct scattering problem for the NLS equation (1) is solved for a particular initial data $u(x, 0) = \text{sech } x$ with the condition $\kappa \geq 2$ [13]. A Cauchy problem constructed on the generalized function type initial data is solved in a certain algebra of some particular generalized functions [14].

Solitons of self-focusing form of the NLS equation are in different forms with various characteristic properties. The envelope soliton decays zero as a Ma soliton decays to the uniform solution [5]. When the real components of the eigenvalues are equal, bi-soliton type solution whose velocity depends on these eigenvalues can be derived. On the other hand, a dark soliton decays to a uniform solution of the defocussing NLS equation [15]. Peregrine's study [5] also suggests a new type analytical solution in rational form describing an isolated amplitude peak. Some exact solutions expressed in terms of some trigonometric and hyperbolic functions can be constructed by He's Lindstedt-Poincaré method in the modified form [16]. The complex tangent function is capable to find some exact traveling wave solutions in the hyperbolic function form as some ansatzes defined as the multiplication of tanh and exponential functions leads some explicit exact solutions [17].

In addition to many analytical or theoretical studies on the NLS equation, various numerical methods have been derived for the analytical or non-analytical solutions. Taha proposes some local and global methods for the numerical solution to an initial boundary value problem whose solution is a model for the motion of an single initial pulse. He compares his results with the results obtained by some classical numerical methods covering local scheme, pseudospectral and split step Fourier methods [18].

Dereli et al. [19] investigate the motion of single positive soliton and the collision of a couple of positive solitons moving in the opposite directions along the horizontal axis numerically. In the study, the radial basis meshless collocation method in four different radial functions, Gaussian, multiquadric, inverse quadric and inverse multiquadric is implemented. The authors report that the least error, accordingly, the best results are generated by the Gaussian functions.

Some finite difference methods covering linearized Crank-Nicolson scheme are derived for solutions of the three model problems for the inhomogeneous NLS equation by Chang et al. [20]. A comparison with Hopscotch-type methods, split step Fourier and spectral schemes indicates that the newly proposed method is efficient and robust.

Quadratic B-spline finite element method [21] is another significant study in the related literature. Dag obtains the numerical simulations of various initial boundary value problems covering propagation of single soliton, bound state of solitons and wave birth models for both standing and traveling initial pulses. This paper is one of the earlier numerical studies dealing with the NLS equation. Gardner et al. [22] solve different initial-boundary value analytical and non-analytical problems with various characteristics for the cubic NLS equation by the cubic B-spline finite elements. The Taylor collocation method based on the quintic B-splines is derived for the similar problems of the cubic NLS equation [23].

Bound states of the NLS equation are deeply investigated by using L^2 -Galerkin with product approximation and Ablowitz & Ladik integrable finite difference methods in [24]. Twizell et al. [25] reduce some initial-boundary value problems for the nonlinear cubic NLS equation to a linear initial value problems of order one by a family of finite difference techniques. They also examined the truncation error, stability and convergence properties of the proposed methods in details. Moreover, they suggest a report explaining the effects of the coefficients to the error between the numerical and the analytical solutions.

Some wave birth models with small dispersion parameters to the focusing NLS equation is studied in details with a second order semi-implicit adaptive moving mesh method [26].

Differential quadrature methods based on cosine expansion have been successfully implemented to five analytical or non-analytical problems for the NLS equation [27]. Motion of single soliton, collision of two positive solitons traveling in the opposite directions along the horizontal axis, bound state of solitons, wave birth by standing or traveling single solitary wave are simulated successfully. The conservation laws are in a good agreement with the theoretical aspects as expected. In the same year, Korkmaz and Dag [28] announce that they solve the same equation with a variation of the differential quadrature method. This time, they use Lagrange interpolation polynomials as basis in the space discretization but do not change the time integration technique.

Different from the last two studies, we derive differential quadrature method based on sine cardinal functions combined with a family of time integration techniques in different classes for the numerical solutions of some initial boundary value problems to cubic NLS equation. The assumption $u(x, t) = f(x, t) + ig(x, t)$, $i = \sqrt{-1}$ reduces the cubic NLS equation (1) to a coupled system of ODEs

$$\begin{aligned} g_t &= f_{xx} + \kappa(f^2 + g^2)f \\ f_t &= -g_{xx} - \kappa(f^2 + g^2)g \end{aligned} \tag{2}$$

where $f = f(x, t)$ and $g = g(x, t)$ are real functions. The artificial homogeneous Dirichlet boundary data at both ends are completely compatible to the chosen

models having physical requirement that $u(x, t) \rightarrow 0$ as $|x| \rightarrow \infty$. Since $u(x, t) = f(x, t) + ig(x, t)$, the boundary conditions for the system (2) are adapted as

$$\begin{aligned} f(a, t) &= 0, f(b, t) = 0 \\ g(a, t) &= 0, g(b, t) = 0 \end{aligned} \quad (3)$$

2 Design of the Method

Consider a sufficiently smooth function $u = u(x, t)$ over a finite interval $[a, b]$. Even though the function u is function of two variables, the second variable t (the time variable through the study) is assumed to be fixed while approximating to the derivatives with respect to the space variable x . Thus, r .th order the derivative of the function u with respect to x is approximated by the finite weighted sum of all functional values in the interval $[a, b]$. Let $[a, b]$ be partitioned as $P : a = x_0 < x_1 < \dots < x_N = b$. One should mention that each grid can be written in terms of grid size and the subscript of the grid as $x_m = m\Delta x$. The definition of the differential quadrature derivative approximation of $u(x, t)$ at a distinct grid point x_m is

$$\left. \frac{\partial^r u(x, t)}{\partial x^r} \right|_{x=x_m} = \sum_{j=0}^N w_{m,j}^{(r)} u(x_j, t), \quad 0 \leq m \leq N \quad (4)$$

where $w_{m,j}^{(r)}$ is the weight of $u(x_j, t)$ for the r .th order derivative approximation of the function $u(x, t)$ at the internal grid point x_i [29]. The significant point of the approximation is the determination of the weights $w_{m,j}^{(r)}$. Once, they are determined, the approximation (4) is directly substituted instead of the related derivatives in the differential equation. Since there may exist different basis function sets spanning the same function or vector space, those basis all enable to determine the weights [29–34]. In this study, the weights are calculated by the set of sine cardinal functions spanning the problem interval.

A sine cardinal function set $\{T_m(x)\}_{m=0}^N$ with elements

$$T_m(x) = \begin{cases} \frac{\sin([\frac{x - m\Delta x}{\Delta x}] \pi)}{[\frac{x - m\Delta x}{\Delta x}] \pi} & , \quad x \neq m\Delta x \\ 1 & , \quad x = m\Delta x \end{cases} \quad (5)$$

constitutes a basis for the functions defined in $[a, b]$ where Δx is the equal grid size [35–38]. A sine cardinal function value at a grid in $[a, b]$ can be calculated easily as

$$T_m(x_j) = \delta_{mj} \quad (6)$$

where δ_{mj} is the Kronecker operator [38]. The function $C(u)(x)$ approximated by an infinite convergent series

$$C(u)(x) = \sum_{m=-\infty}^{\infty} u(m\Delta x)T_m(x) \quad (7)$$

is named the cardinal of u on $(-\infty, \infty)$ and it interpolates u at the points that are integer multiple of Δx [39].

The lowest ordered two derivatives of a sine cardinal function $T_m(x)$ are calculated in an explicit form as:

$$T'_m(x) = \begin{cases} \frac{\frac{\pi}{\Delta x}(x - m\Delta x) \cos \frac{x - m\Delta x}{\Delta x} \pi - \sin \frac{x - m\Delta x}{\Delta x} \pi}{\frac{\pi}{\Delta x}(x - m\Delta x)^2} & , \quad x \neq m\Delta x \\ 0 & , \quad x = m\Delta x \end{cases} \quad (8)$$

$$T''_m(x) = \begin{cases} \frac{-\frac{\pi}{\Delta x} \sin \frac{x - m\Delta x}{\Delta x} \pi}{x - m\Delta x} - \frac{2 \cos \frac{x - m\Delta x}{\Delta x} \pi}{(x - m\Delta x)^2} + \frac{2 \sin \frac{x - m\Delta x}{\Delta x} \pi}{\frac{\pi}{\Delta x}(x - m\Delta x)^3} & , \quad x \neq m\Delta x \\ -\frac{\pi^2}{3\Delta x^2} & , \quad x = m\Delta x \end{cases} \quad (9)$$

In order to calculate the weights $w_{mj}^{(2)}$ of the approximation to second order derivative terms f_{xx} and g_{xx} , we substitute each sine cardinal function into the differential quadrature approximation equation (4) for $r = 2$.

Assume that $m = 0$. That means all $N + 1$ weights $w_{0j}^{(2)}$ are determined by substituting each sine cardinal function $T_m(x)$ and its second order derivative into (4). Although its not necessary to follow an order, all calculations are completed in an order for convenience and simplicity. Substituting $T_0(x)$ and its second order derivative into the (4) gives

$$\begin{aligned} T''_0(x_0) &= \sum_{j=0}^N w_{0j}^{(2)} T_0(x_j) \\ &= w_{00}^{(2)} T_0(x_0) + w_{01}^{(2)} T_0(x_1) + \dots + w_{0N}^{(2)} T_0(x_N) \\ &= w_{00}^{(2)} \delta_{00} + w_{01}^{(2)} \delta_{01} + \dots + w_{0N}^{(2)} \delta_{0N} \\ \frac{-\pi^2}{3\Delta x^2} &= w_{00}^{(2)} \end{aligned} \quad (10)$$

The same methodology can be used to find the weight $w_{01}^{(2)}$ as

$$\begin{aligned}
T_1''(x_0) &= \sum_{j=0}^N w_{0j}^{(2)} T_0(x_j) \\
&= w_{00}^{(2)} T_1(x_0) + w_{02}^{(2)} T_1(x_1) + \dots + w_{0N}^{(2)} T_1(x_N) \\
&= w_{00}^{(2)} \delta_{10} + w_{01}^{(2)} \delta_{11} + \dots + w_{0N}^{(2)} \delta_{1N} \\
-\frac{2 \cos\left(\frac{x_0 - \Delta x}{\Delta x} \pi\right)}{(x_0 - \Delta x)^2} &= w_{01}^{(2)} \\
-\frac{2 \cos\left(\frac{0\Delta x - \Delta x}{\Delta x} \pi\right)}{(0\Delta x - \Delta x)^2} &= w_{01}^{(2)} \\
-\frac{2 \cos((0-1)\pi)}{(0-1)^2 \Delta x^2} &= w_{01}^{(2)} \\
\frac{2(-1)^{(0-1+1)}}{(0-1)^2 \Delta x^2} &= w_{01}^{(2)}
\end{aligned} \tag{11}$$

where the identity $\cos(k\pi) = (-1)^k$ is used to rearrange the left hand side of the equation. This procedure can be generalized for any weight $w_{0m}^{(2)}$ related to the point x_0 originated from the point x_m by using the basis $T_m(x)$ as

$$\begin{aligned}
T_m''(x_0) &= \sum_{j=0}^N w_{0j}^{(2)} T_m(x_j) \\
&= w_{00}^{(2)} T_m(x_0) + w_{01}^{(2)} T_m(x_1) + \dots + w_{0m}^{(2)} T_m(x_m) + \dots + w_{0N}^{(2)} T_m(x_N) \\
&= w_{00}^{(2)} \delta_{m0} + w_{01}^{(2)} \delta_{m1} + \dots + w_{0m}^{(2)} \delta_{mm} + \dots + w_{0N}^{(2)} \delta_{mN} \\
\frac{2(-1)^{(0-m+1)}}{(0-m)^2 \Delta x^2} &= w_{0m}^{(2)}
\end{aligned} \tag{12}$$

This explicit form can be extended for an arbitrary weight $w_{mj}^{(2)}$, related to the point x_m originated from x_j , as

$$w_{mj}^{(2)} = \frac{2(-1)^{m-j+1}}{\Delta x^2 (m-j)^2} \tag{13}$$

when $m \neq j$, and

$$w_{mm}^{(2)} = -\frac{\pi^2}{3\Delta x^2} \tag{14}$$

when $m = j$. This explicit formulation of the weights are used some earlier studies for various problems [40, 41].

Even though the determination of only the second derivatives weights is sufficient due to the structure of the NLS equation, the weights $w_{mj}^{(1)}$ should also be calculated to compute the conservation law C_3 having first order derivative in. Thus, we start by letting $r = 1$ in the (4). In order to determine the weights $w_{0j}^{(1)}$, assume that $m = 0$ initially. Substituting the first element $T_0(x)$ of the basis functions set into the differential quadrature approximation (4) gives

$$\begin{aligned} T_0'(x_0) &= \sum_{j=0}^N w_{0j}^{(1)} T_0(x_j) \\ &= w_{00}^{(1)} T_0(x_0) + w_{01}^{(1)} T_0(x_1) + \dots + w_{0N}^{(1)} T_0(x_N) \\ &= w_{00}^{(1)} \delta_{00} + w_{01}^{(1)} \delta_{01} + \dots + w_{0N}^{(1)} \delta_{0N} \\ 0 &= w_{00}^{(1)} \end{aligned}$$

Similarly, substituting the next basis function $T_1(x)$ into the differential quadrature approximation (4) yields

$$\begin{aligned} T_1'(x_0) &= \sum_{j=0}^N w_{0j}^{(1)} T_1(x_j) \\ &= w_{00}^{(1)} T_1(x_0) + w_{01}^{(1)} T_1(x_1) + \dots + w_{0N}^{(1)} T_1(x_N) \\ &= w_{00}^{(1)} \delta_{10} + w_{01}^{(1)} \delta_{11} + \dots + w_{0N}^{(1)} \delta_{1N} \\ \frac{\frac{\pi}{\Delta x} (x_0 - 1\Delta x) \cos \frac{x_0 - 1\Delta x}{\Delta x} \pi - \sin \frac{x_0 - 1\Delta x}{\Delta x} \pi}{\frac{\pi}{\Delta x} (x_0 - 1\Delta x)^2} &= w_{01}^{(1)} \\ \frac{\frac{\pi}{\Delta x} (0\Delta x - 1\Delta x) \cos \frac{0\Delta x - 1\Delta x}{\Delta x} \pi - \sin \frac{0\Delta x - 1\Delta x}{\Delta x} \pi}{\frac{\pi}{\Delta x} (0\Delta x - 1\Delta x)^2} &= w_{01}^{(1)} \\ \frac{(0 - 1) \cos (0 - 1)\pi - \sin (0 - 1)\pi}{(0 - 1)^2 (\Delta x)^2} &= w_{01}^{(1)} \\ \frac{\cos (0 - 1)\pi}{(0 - 1)\Delta x} &= w_{01}^{(1)} \\ \frac{(-1)^{(0-1)}}{(0 - 1)\Delta x} &= w_{01}^{(1)} \end{aligned}$$

where $\cos (0 - 1)\pi$ is replaced by $(-1)^{0-1}$. Substituting the basis function $T_m(x)$

into (4) leads

$$\begin{aligned}
T'_2(x_0) &= \sum_{j=0}^N w_{0j}^{(1)} T_2(x_j) \\
&= w_{00}^{(1)} T_1(x_0) + w_{02}^{(1)} T_1(x_1) + \dots + w_{0N}^{(1)} T_1(x_N) \\
&= w_{00}^{(1)} \delta_{20} + w_{01}^{(1)} \delta_{21} + w_{02}^{(1)} \delta_{22} \dots + w_{0N}^{(1)} \delta_{1N} \\
&= \frac{\frac{\pi}{\Delta x} (x_0 - 2\Delta x) \cos \frac{x_0 - 2\Delta x}{\Delta x} \pi - \sin \frac{x_0 - 2\Delta x}{\Delta x} \pi}{\frac{\pi}{\Delta x} (x_0 - 2\Delta x)^2} = w_{02}^{(1)} \\
&= \frac{\frac{\pi}{\Delta x} (0\Delta x - 2\Delta x) \cos \frac{0\Delta x - 2\Delta x}{\Delta x} \pi - \sin \frac{0\Delta x - 2\Delta x}{\Delta x} \pi}{\frac{\pi}{\Delta x} (0\Delta x - 2\Delta x)^2} = w_{02}^{(1)} \\
&= \frac{(0 - 2) \cos(0 - 2)\pi - \sin(0 - 2)\pi}{(0 - 2)^2 (\Delta x)^2} = w_{02}^{(1)} \\
&= \frac{\cos(0 - 2)\pi}{(0 - 2)\Delta x} = w_{02}^{(1)} \\
&= \frac{(-1)^{(0-2)}}{(0 - 2)\Delta x} = w_{02}^{(1)}
\end{aligned}$$

to give the related weight in an explicit form. Following the same methodology leads an explicit formulation for an arbitrary weight $w_{mj}^{(1)}$ as

$$\begin{aligned}
w_{mj}^{(1)} &= \frac{(-1)^{m-j}}{\Delta x(m-j)}, m \neq j \\
w_{mm}^{(1)} &= 0
\end{aligned}$$

for the weights $w_{mj}^{(1)}$ that are related to the grid x_m .

3 Discretization, Implementation of Boundary Conditions and Time integration

Approximating the derivative terms in the coupled system of partial differential equations (2) gives the ordinary system of equations

$$\begin{aligned}
\left. \frac{\partial g(x, t)}{\partial t} \right|_{x=x_m} &= \sum_{j=0}^N w_{m,j}^{(2)} f(x_j, t) + \kappa (f^2(x_m, t) + g^2(x_m, t)) f(x_m, t) \\
\left. \frac{\partial f(x, t)}{\partial t} \right|_{x=x_m} &= - \sum_{j=0}^N w_{m,j}^{(2)} g(x_j, t) - \kappa (f^2(x_m, t) + g^2(x_m, t)) g(x_m, t) \\
m &= 0, 1, \dots, N
\end{aligned} \tag{15}$$

related to each grid point x_m . Implementation of the homogeneous Dirichlet boundary conditions (3) converts the system (15) to

$$\begin{aligned} \left. \frac{\partial g(x, t)}{\partial t} \right|_{x=x_m} &= \sum_{j=1}^{N-1} w_{m,j}^{(2)} f(x_j, t) + \kappa (f^2(x_m, t) + g^2(x_m, t)) f(x_m, t) \\ \left. \frac{\partial f(x, t)}{\partial t} \right|_{x=x_m} &= - \sum_{j=1}^{N-1} w_{m,j}^{(2)} g(x_j, t) - \kappa (f^2(x_m, t) + g^2(x_m, t)) g(x_m, t) \end{aligned} \quad (16)$$

$$m = 1, 2, \dots, N - 1$$

In order to integrate the space discretized system (16), a bunch of methods of various orders covering Heun's method(HEUN), the classical Runge-Kutta methods of order from two to four (RK2,RK3,RK4) and some variations of higher order Runge-Kutta methods such as the Runge-Kutta-Fehlberg (RKF) and the Cash-Karp (CK) methods are used. The solutions are computed for different choices of discretization parameters Δx and Δt without any linearization.

4 On the Matrix Stability of the Proposed Methods

In this part, some basic concepts related to the stability of explicit Runge-Kutta methods are presented. The stability regions for each method used in this study are graphed in order to indicate the relation between the eigenvalue distribution and the stability of the method. The spectrum of the coefficient matrix gives the idea to choose appropriate Δt to provide the stability condition. The stability region of a Runge-Kutta method of order p depends on the stability polynomial $|S(\lambda\Delta t)| < 1$ defined as

$$S(\lambda\Delta t) = \sum_{s=0}^p \frac{(\lambda\Delta t)^s}{s!} \quad (17)$$

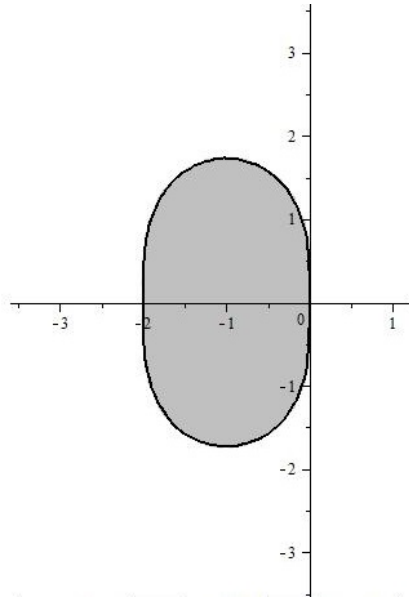
since the common approximation in the Runge-Kutta methods are of the form

$$y_{n+1} = S(\lambda\Delta t)y_n \quad (18)$$

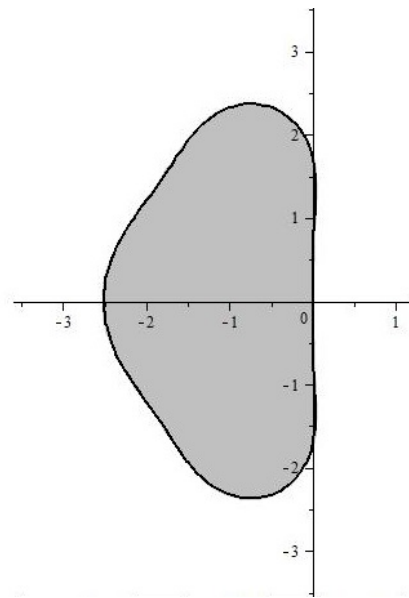
for the differential equation

$$\frac{dy}{dt} = \lambda y \quad (19)$$

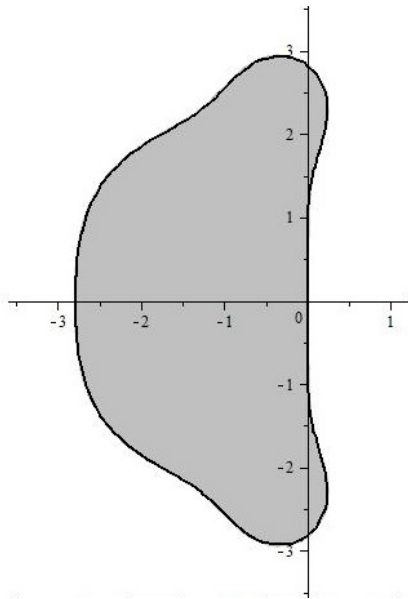
The stability regions of the Runge-Kutta methods of orders from two to five are plotted in Fig 1(a)-Fig 1(d).



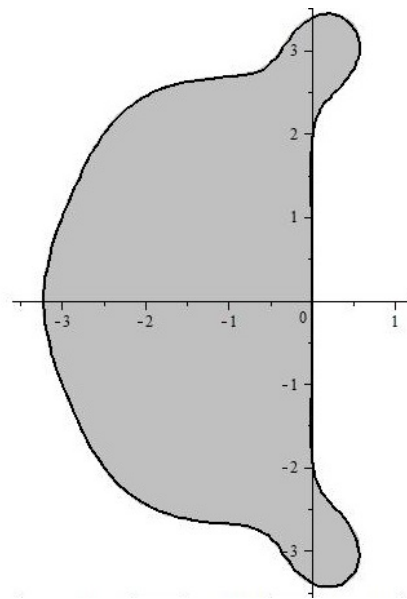
(a) Order 2



(b) Order 3



(c) Order 4



(d) Order 5

Figure 1: Stability regions for Runge-Kutta methods in the complex plane

Now consider the linear equation system of order one such that

$$\frac{d\mathbf{y}}{dt} = \mathbf{B}\mathbf{y} \quad (20)$$

where \mathbf{B} is the coefficient matrix with constant coefficients, $\mathbf{y} = [y_1, y_2, \dots, y_N]^T$. The stability of this system is dependent on the eigenvalue distribution of the coefficient matrix \mathbf{B} .

The space discretized system (16) can be written in the matrix format as

$$\begin{bmatrix} g_1(t) \\ g_2(t) \\ \vdots \\ g_{N-1}(t) \\ f_1(t) \\ f_2(t) \\ \vdots \\ f_{N-1}(t) \end{bmatrix}_t = \begin{bmatrix} \mathbf{0} & \mathbf{A} \\ -\mathbf{A} & \mathbf{0} \end{bmatrix} \begin{bmatrix} g_1(t) \\ g_2(t) \\ \vdots \\ g_{N-1}(t) \\ f_1(t) \\ f_2(t) \\ \vdots \\ f_{N-1}(t) \end{bmatrix} \quad (21)$$

$$\mathbf{A} = \begin{bmatrix} w_{11}^{(2)} + \kappa\tilde{\kappa}_1 & w_{12}^{(2)} & \dots & w_{1N-1}^{(2)} \\ w_{21}^{(2)} & w_{22}^{(2)} + \kappa\tilde{\kappa}_2 & \dots & w_{2N-1}^{(2)} \\ \vdots & \ddots & \ddots & \vdots \\ w_{N-11}^{(2)} & w_{N-12}^{(2)} & \dots & w_{N-1N-1}^{(2)} + \kappa\tilde{\kappa}_{N-1} \end{bmatrix} \quad (22)$$

where $\tilde{\kappa}_m = f_m^2 + g_m^2$ is assumed locally constant and f_m and g_m stand for $f(x_m, t)$ and $g(x_m, t)$, respectively. We investigate the eigenvalues of the coefficient matrix (21) by using the initial values of f_m and g_m for each test problem given in the following.

5 Numerical Examples

In this section of the study, some analytical and non-analytical initial-boundary value problems are considered. The error between the numerical and the analytical solutions is determined by using the discrete maximum error norm at the time t defined as

$$L_\infty(t) = \max_m |U_m - u_m|$$

where u_m and U_m are the analytical and numerical solutions at $x = x_m$, respectively.

The lowest two conservation laws for the NLS equation defined as

$$\begin{aligned} C_1 &= \int_{-\infty}^{\infty} |u|^2 dx \\ C_3 &= \int_{-\infty}^{\infty} \left[|u_x|^2 - \frac{1}{2} \kappa |u|^4 \right] dx \end{aligned} \quad (23)$$

are expected to remain constant as time proceeds [1]. Even though C_2 and C_4 are also defined in the same paper, we do not calculate them here due to having complex components inside the integrals. Reporting the absolute relative change of the conservation laws at a specific time t defined as

$$C(C_\eta(t)) = \left| \frac{C_\eta(t) - C_\eta(0)}{C_\eta(0)} \right|, \eta = 1, 3 \quad (24)$$

where $C_\eta(0), \eta = 1, 3$ denote the determined conservation law values initially can more useful to observe the preservation of the conservation laws.

5.1 Propagation of a Single Soliton

The soliton solutions of the NLS is completely different from the solitons of KdV equation since they include both exponential and hyperbolic functions. These soliton solutions of the form

$$u(x, t) = \alpha \sqrt{\frac{2}{\kappa}} \exp i \left[\frac{cx}{2} - \frac{(c^2 - \alpha^2)t}{4} \right] \text{sech } \alpha(x - ct) \quad (25)$$

comes into existence when the nonlinear and the dispersion terms are balanced completely. In this solution, c stands for the velocity of the propagating soliton. In order to enable a comparison with some earlier studies, the parameters are selected as $c = 4$, $\kappa = 2$ and $\alpha = 1$. Thus, the resultant envelop solution

$$|u(x, t)| = \text{sech}(x - 4t) \quad (26)$$

represents a single soliton of constant speed 4 propagating along the x -axis with height 1. Various discretization parameters are used for the numerical illustrations in the experiment interval $[-20, 24]$ up to the time $t = 1$. The simulation of the propagation of the single soliton is depicted in Fig 2.

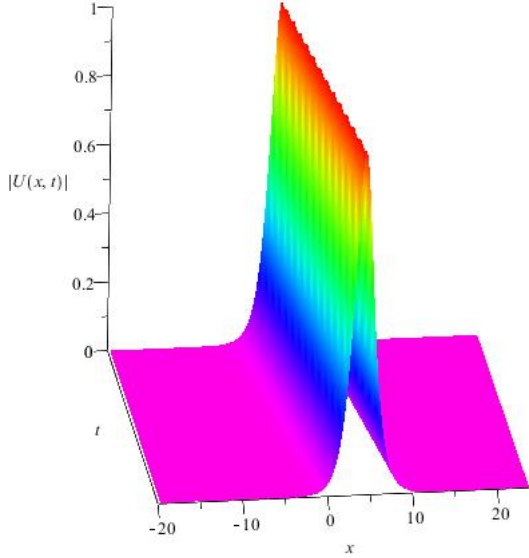


Figure 2: Propagation of single soliton simulation achieved by using parameters $\Delta t = 0.0001$ and $\Delta x = 0.1$

The time integration is carried out by using various techniques of orders from lower ones to higher ones. The discrete maximum error norms are tabulated in Table 1 for each choice of methods, space and time step sizes.

The initial values of conservation laws C_1 and C_3 are determined as 2 and 7.333333333 analytically. A comparison of discrete maximum errors and the absolute relative changes of the conservation laws are documented in Table 1.

When $\Delta t = 0.1$, all time integration techniques from HEUN to CK fail independent on the space grid sizes $\Delta x = 0.3125$ and $\Delta x = 0.1$ to generate the numerical solutions due to not satisfying the stability conditions. A discussion on the details of the stability is given in the following parts of this section. Since both HEUN and RK2 are of order two, the results generated by both methods are almost at the same digit-accuracy. When $\Delta x = 0.3125$, the accuracies are determined in three, five and six decimal digits dependent on the size of time step 0.01, 0.001 and 0.0001, respectively. Unfortunately, the decrease of the grid size to 0.1 unbalances the stability for $\Delta t = 0.1, 0.01, 0.001$. This balance is caught again with higher accuracy for $\Delta t = 0.0001$. The accuracy reaches seven decimal digits with this choice of Δt .

The RK3 method gives five decimal-digit accuracy with $\Delta x = 0.3125$ and $\Delta t = 0.01$. Reducing Δt to 0.001 and 0.0001 improves results to six decimal-digit accuracy. The decrease of Δx to 0.1 gives no results when $\Delta t = 0.1, 0.01$ but the

choice of Δt as 0.001 and 0.0001 gives eight and nine decimal-digit accuracies, respectively.

The RK4, the RKF and the CK methods are accurate at six decimal digits with the discretization parameters $\Delta x = 0.3125$ and $\Delta t = 0.01, 0.001, 0.0001$. When the discretization parameters are chosen as $\Delta x = 0.1$ and $\Delta t = 0.001, 0.0001$, nine decimal-digit accuracy are obtained in the results.

The comparison with the earlier works indicates that the proposed methods solve this initial boundary value problem with acceptably higher accuracy. The proposed methods give better results than the results of the B-spline FEM [21], the B-spline Collocation [22] and the RBF methods [19]. Even though the results of CDQ [27] appear worse than other the present results in many cases the authors of that study explain the high error due to the forced boundary effect in $[-20, 20]$. The change of the problem interval from $[-20, 20]$ to $[-20, 24]$ decreases the forced boundary effect on the accuracy of the results when Dirichlet conditions are used [27]. The results of the PDQ [28] are acceptably accurate but not better than the present results in many cases.

The conservation laws calculated by using each numerical method are indicators of highly accurate results. The relative absolute changes decreases depending on the accuracy and the order of the method. Particularly, the absolute relative changes decreases below 10^{-10} when the stable higher order methods are used. The observations are in a good agreement with the theoretical expectations and the results reported in [27, 28].

The stability analysis of the proposed methods depends on the eigenvalue distribution of the coefficient matrix given in the previous section. Assuming the real and the complex components of the solution are locally constant converts the system to a linear system with constant coefficient matrix \mathbf{B} . The spectrum of this coefficient matrix gives the information to control the size of Δt for the stability of the method. When Δx is chosen as 0.3125, the complex components of the eigenvalues are larger than 100 in absolute value, Fig 3(a). The choice of the time step size Δt should squeeze the value of the multiplication of each eigenvalue λ_i and Δt to the regions given in Fig 1(a)-Fig 1(d) correspond to the order. Similar conclusion can be written for the choice of $\Delta x = 0.1$ by commenting on Fig 3(b). Since some of the complex components of the eigenvalues are greater than 900 in absolute value, the stability forces Δt to be chosen smaller. This perspective explains why time integration techniques fail to solve the problem.

Table 1: Comparison of the results with the results of some earlier works

Method	Δx	Δt	$L_\infty(1)$	$C(C_1(1))$	$C(C_3(1))$	
HEUN (present)	0.3125	0.1	∞	∞	∞	
		0.01	2.629×10^{-3}	1.527×10^{-4}	9.563×10^{-4}	
		0.001	2.494×10^{-5}	1.215×10^{-7}	2.360×10^{-7}	
		0.0001	1.378×10^{-6}	5.000×10^{-10}	1.363×10^{-9}	
	0.1	0.1	∞	∞	∞	
		0.01	∞	∞	∞	
		0.001	∞	∞	∞	
		0.0001	2.471×10^{-7}	$< 10^{-10}$	2.727×10^{-10}	
	RK2 (present)	0.3125	0.1	∞	∞	∞
			0.01	2.629×10^{-3}	1.527×10^{-4}	9.563×10^{-4}
0.001			2.494×10^{-5}	1.215×10^{-7}	2.360×10^{-7}	
0.0001			4.837×10^{-6}	5.000×10^{-10}	1.363×10^{-9}	
0.1		0.1	∞	∞	∞	
		0.01	∞	∞	∞	
		0.001	∞	∞	∞	
		0.0001	2.471×10^{-7}	$< 10^{-10}$	2.727×10^{-10}	
RK3 (present)		0.3125	0.1	∞	∞	∞
			0.01	7.560×10^{-5}	4.064×10^{-5}	7.883×10^{-5}
	0.001		1.378×10^{-6}	4.050×10^{-8}	7.854×10^{-8}	
	0.0001		1.378×10^{-6}	5.000×10^{-10}	4.090×10^{-10}	
	0.1	0.1	∞	∞	∞	
		0.01	∞	∞	∞	
		0.001	7.510×10^{-8}	4.100×10^{-8}	7.854×10^{-8}	
		0.0001	2.800×10^{-9}	5.000×10^{-10}	8.181×10^{-10}	
	RK4 (present)	0.3125	0.1	∞	∞	∞
			0.01	2.092×10^{-6}	4.500×10^{-8}	1.262×10^{-7}
0.001			1.378×10^{-6}	5.000×10^{-10}	1.227×10^{-9}	
0.0001			1.378×10^{-6}	5.000×10^{-10}	1.227×10^{-9}	
0.1		0.1	∞	∞	∞	
		0.01	∞	∞	∞	
		0.001	2.814×10^{-9}	$< 10^{-10}$	$< 10^{-10}$	
		0.0001	2.805×10^{-9}	$< 10^{-10}$	$< 10^{-10}$	
RKF (present)		0.3125	0.1	∞	∞	∞
			0.01	1.380×10^{-6}	6.000×10^{-9}	4.750×10^{-8}
	0.001		1.378×10^{-6}	$< 10^{-10}$	$< 10^{-10}$	
	0.0001		1.378×10^{-6}	$< 10^{-10}$	$< 10^{-10}$	
	0.1	0.1	∞	∞	∞	
		0.01	∞	∞	∞	
		0.001	2.803×10^{-9}	$< 10^{-10}$	$< 10^{-10}$	
		0.0001	2.805×10^{-9}	$< 10^{-10}$	$< 10^{-10}$	
	CK (present)	0.3125	0.1	∞	∞	∞
			0.01	1.379×10^{-6}	1.190×10^{-9}	1.808×10^{-9}
0.001			1.378×10^{-6}	$< 10^{-10}$	$< 10^{-10}$	
0.0001			1.378×10^{-6}	$< 10^{-10}$	$< 10^{-10}$	
0.1		0.1	∞	∞	∞	
		0.01	∞	∞	∞	
		0.001	2.804×10^{-9}	$< 10^{-10}$	$< 10^{-10}$	
		0.0001	2.805×10^{-9}	$< 10^{-10}$	$< 10^{-10}$	
CDQ [27]		0.3125	0.025	5.562×10^{-5}	4.380×10^{-6}	1.214×10^{-5}
			0.01	2.089×10^{-6}	4.512×10^{-8}	1.253×10^{-7}
	0.125	0.0025	1.557×10^{-6}	4.412×10^{-11}	1.226×10^{-10}	
		0.001	1.550×10^{-7}	4.541×10^{-13}	1.266×10^{-12}	
PDQ [28]	0.3125	0.02	2.531×10^{-5}	1.440×10^{-6}	3.941×10^{-6}	
	0.1	0.0025	1.932×10^{-7}	5.222×10^{-11}	2.930×10^{-9}	
B-spline FEM [21]	0.3125	0.02	0.002	6.600×10^{-6}	3.417×10^{-4}	
	0.05	0.005	3.000×10^{-4}	$< 10^{-8}$	6.000×10^{-7}	
B-spline Collocation [22]	0.05	0.005	0.008	$< 10^{-6}$	$< 10^{-6}$	
	0.03	0.005	0.002	$< 10^{-6}$	$< 10^{-6}$	
RBF Method G [19]	0.3125	0.001	2.800×10^{-5}			
RBF Method MQ [19]	0.3125	0.001	2.165×10^{-3}			
RBF Method IMQ [19]	0.3125	0.001	4.860×10^{-4}			
RBF Method IQ [19]	0.3125	0.001	5.652×10^{-3}			

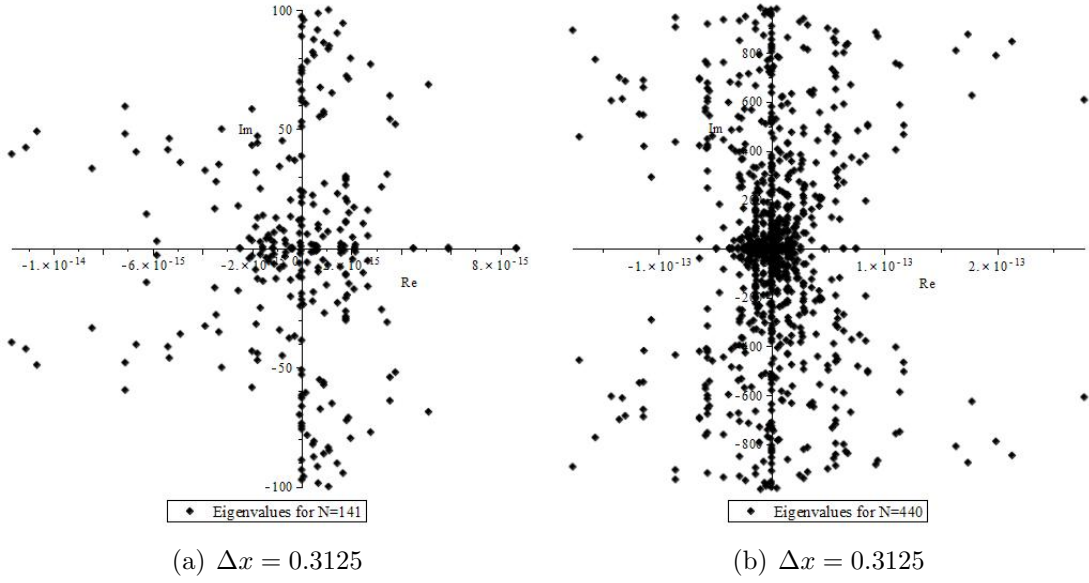


Figure 3: The eigenvalue distributions for propagation of a single soliton

5.2 Collision of Two Positive Solitary Waves Moving in the Opposite Directions

The collision of two positive solitary waves moving in the opposite directions along the x -axis is modeled by the initial data

$$u(x, 0) = \sum_{j=1}^2 u_j(x, 0)$$

where

$$u_j(x, 0) = \beta_j \sqrt{\frac{2}{\kappa}} \exp \left(i \frac{1}{2} c_j (x - \hat{x}_j) \right) \operatorname{sech} \beta_j (x - \hat{x}_j), \quad j = 1, 2$$

where \hat{x}_j stands for the peak positions of the solitary waves initially. The experiment is completed with the appropriate parameters $\kappa = 2$, $\beta_j = 1, j = 1, 2$, $c_1 = 4$ and $c_2 = -4$ used in the previous studies [21, 22, 27, 28]. The peaks of the well separated two positive solitary waves are sited to $x = -10$ and $x = 10$ initially by choosing $\hat{x}_1 = -10$ and $\hat{x}_2 = 10$, respectively. The numerical solutions are computed with the discretization parameters $\Delta x = 0.25$ and $\Delta t = 0.005$ in the artificial domain $[-20, 20]$, Fig 4. All routines are run up to time $t = 5$ to observe the separation clearly after the collision. This choice of simulation ending time

restricts both waves to hit the ends of artificial interval, too. The homogeneous Dirichlet boundary conditions are used to provide the compatibility with theory. Both solitary waves of unit height initially move towards each other due to the difference in the sign of c_1 and c_2 . The collision starts as time proceeds and can be observable clearly around the time $t = 2$. When the time is $t = 2.5$, the height of the joint waves exceeds 1.9 because the structure of the solution is sum of two positive waves. Both waves keep moving along their own ways and separate from each other as time proceeds. After full separation, both waves turn their initial shapes and heights. Each one takes the initial position of the other one owing to their constant velocities 4 when the time reaches $t = 5$.

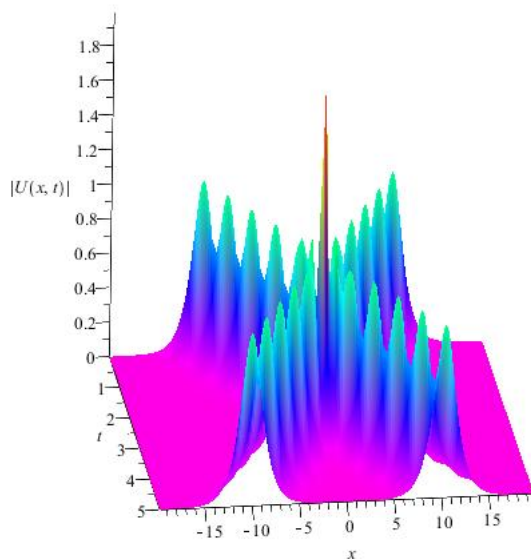


Figure 4: Collision of two positive solitary waves propagating in the opposite directions

The HEUN and the RK2 both fail to simulate the solutions with those discretization parameters. The analytical values of the conservation laws are $C_1 = 4$ and $C_3 = 14.66666667$ initially. The absolute relative changes of the conservation laws are the indicators of the accuracy of the method for this problem due to non existence of the analytical solution. The reported results of absolute relative changes indicate that C_1 and C_3 both change in five decimal digits when the method is RK3, Table 2. The RK4 preserves the conservation laws C_1 and C_3 in nine and eight decimal digits, respectively. The first conservation law is changed relatively in absolute value in ten decimal digits for the methods RKF and CK. The perfor-

mance of RKF is one decimal digit better than eight decimal digits preservation of CK.

Table 2: Absolute relative changes of the conservation laws at $t = 5$

Method	Δx	Δt	$C(C_1(1))$	$C(C_3(1))$
RK3 (present)	0.25	0.005	2.494×10^{-5}	4.793×10^{-5}
RK4 (present)	0.25	0.005	6.250×10^{-9}	3.068×10^{-8}
RKF (present)	0.25	0.005	5.000×10^{-10}	8.863×10^{-9}
CK (present)	0.25	0.005	5.000×10^{-10}	1.090×10^{-8}
PDQ [28]	0.25	0.01	2.215×10^{-7}	4.358×10^{-7}

The eigenvalue distribution related to this problem indicates that the choice of $\Delta t = 0.005$ is not sufficient to carry all $\lambda_j \Delta t$ given in Fig 5 to the stability region Fig 1(a) for the second order methods, HEUN and RK2. The maximum and minimum complex components of all eigenvalues are ± 156.462 and $\pm 156.462 \times 0.005 = \pm 0.782$ is at the outside of the stability region 1(a). However, that choice of Δt is sufficient for the stability of the RK3, the RK4, the RKF and the CK methods.

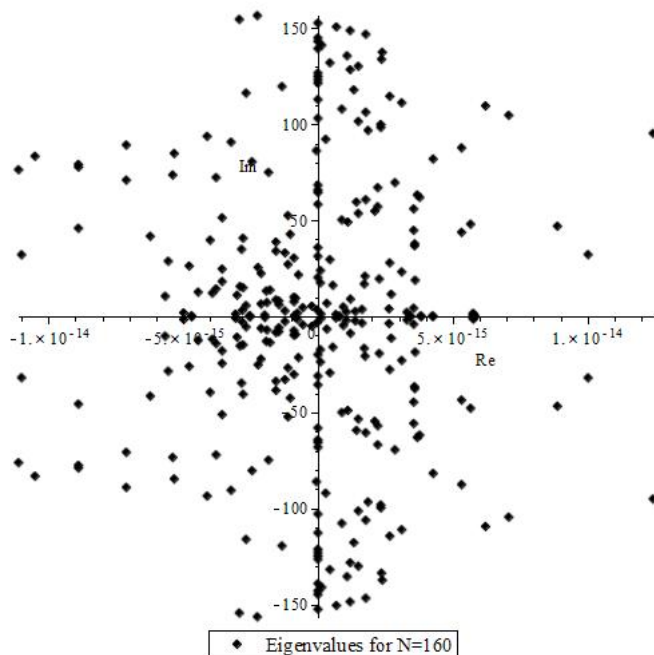


Figure 5: Eigenvalues for the collision of two positive solitaries problem

5.3 Birth of Standing Initial Pulse

The birth of a standing pulse occurs when the integral of initial data is greater than π in the infinite interval. Otherwise the initial pulse fades out as time proceeds. The Maxwellian initial condition [22]

$$u(x, 0) = Ae^{-x^2} \quad (27)$$

is chosen to demonstrate the experiment in the interval $[-45, 45]$. The algorithms are run up to the ending time $t = 6$ with $\kappa = 2$, fixed grid size $\Delta x = 0.5$ and various Δt values. The choice $A = 1$ gives a positive pulse of unit height positioned at $x = 0$ initially but this value of A does not keep the balance in the equation and the initial pulse fades out as time proceeds, Fig 6(a). On the other hand, the choice of A as 1.78 gives an initial pulse of height 1.78. At the earlier times of the motion, the height increases rapidly and gets larger than 2 as giving birth from the both sides of its basis, Fig 6(b). As these two small pulses goes far away from the initial pulse, the height of their mother decreases to below 2. The mother keeps its position, shape and height as the births propagates.

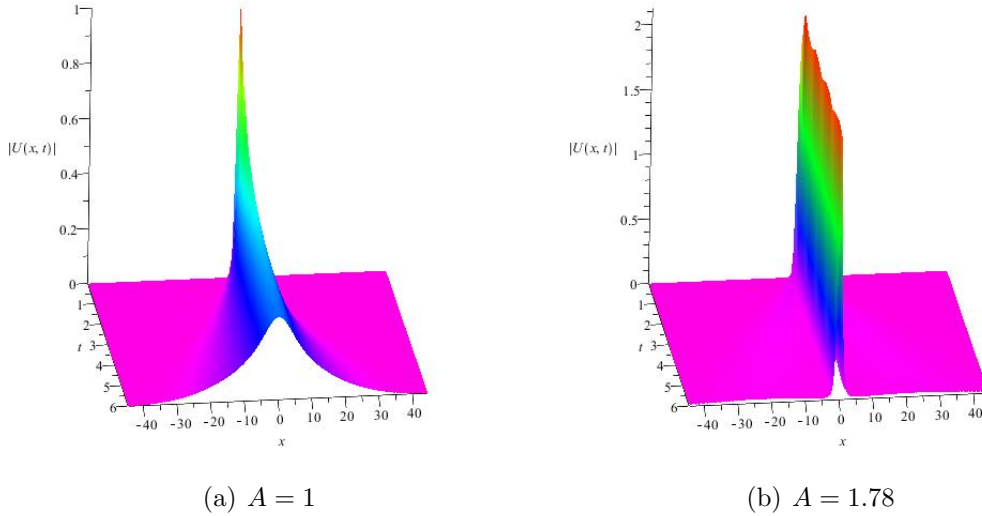


Figure 6: Fade out and birth of a standing initial pulse

The conservation laws are computed from the initial data as $C_1 = A^2\sqrt{\pi/2} \cong 3.97100$ and $C_3 = (\sqrt{\pi}/4)A^2(2\sqrt{2} - \kappa A^2) \cong -4.92653$. The absolute relative changes of the conservation laws are tabulated in Table 3. The discretization parameter choice $\Delta x = 0.5$ and $\Delta t = 0.05$ causes instability for the second and third

order methods. Even though all other choices of the discretization parameters generate acceptably well solutions, the absolute relative change of the third conservation law does not improve for smaller time step sizes. On the contrary, the first conservation law is sensitive to smaller time step sizes when Δx is fixed as 0.5 and improves in digits. The accuracies do not improve too much even the order of the method increases. The comparison with some earlier differential quadrature methods indicates that the present results are satisfactorily well.

Table 3: Absolute relative changes of the conservation laws at $t = 6$ for the birth of standing pulse

Method	Δx	Δt	$C(C_1(6))$	$C(C_3(6))$
HEUN (present)	0.5	0.05	∞	∞
HEUN (present)	0.5	0.005	6.697×10^{-5}	7.708×10^{-4}
HEUN (present)	0.5	0.0005	6.623×10^{-8}	7.362×10^{-5}
RK2 (present)	0.5	0.05	∞	∞
RK2 (present)	0.5	0.005	6.697×10^{-5}	7.708×10^{-4}
RK2 (present)	0.5	0.0005	6.623×10^{-8}	7.362×10^{-5}
RK3 (present)	0.5	0.05	∞	∞
RK3 (present)	0.5	0.005	2.207×10^{-5}	7.163×10^{-4}
RK3 (present)	0.5	0.0005	2.241×10^{-8}	7.361×10^{-4}
RK4 (present)	0.5	0.05	1.267×10^{-4}	4.179×10^{-3}
RK4 (present)	0.5	0.005	2.770×10^{-9}	7.361×10^{-4}
RK4 (present)	0.5	0.0005	7.554×10^{-10}	7.361×10^{-4}
RKF (present)	0.5	0.05	1.571×10^{-4}	4.153×10^{-3}
RKF (present)	0.5	0.005	1.259×10^{-9}	7.361×10^{-4}
RKF (present)	0.5	0.0005	7.554×10^{-10}	7.361×10^{-4}
CK (present)	0.5	0.05	5.548×10^{-5}	8.082×10^{-4}
CK (present)	0.5	0.005	1.259×10^{-9}	7.361×10^{-4}
CK (present)	0.5	0.0005	7.554×10^{-10}	7.361×10^{-4}
CDQ [27]	0.25	0.01	8.836×10^{-8}	3.892×10^{-6}
PDQ [28]	0.25	0.01	6.334×10^{-7}	7.110×10^{-5}

The eigenvalues for $A = 1$ and $A = 1.78$ are graphed in Fig 7(a) and Fig 7(b), respectively. Since the maximum and minimum complex components of all eigenvalues are ± 39.155 , the choice of $\Delta t = 0.05$ or greater values is not sufficient for the stability, Fig 1(a) and Fig 1(b). The multiplication of the maximum(and the minimum) complex component is equal to ± 1.957 . These values are sufficient to satisfy the stability condition for only the higher order methods RK4, RKF and CK.

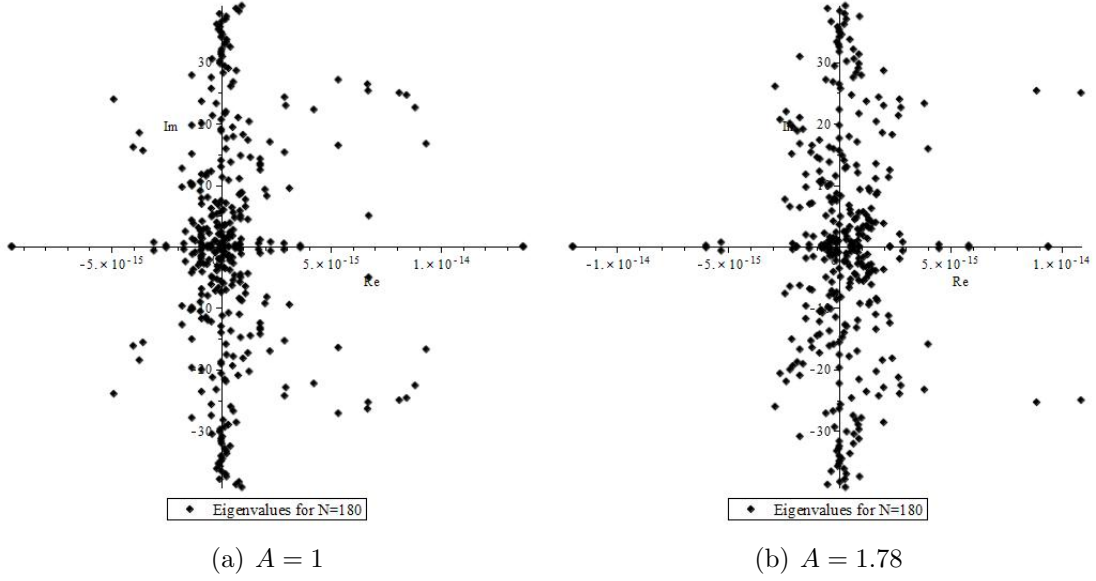


Figure 7: Eigenvalue distribution for the birth of standing initial pulse

5.4 Birth of Propagating Pulse

The birth of propagating pulse problem is a model with the initial data

$$u(x, 0) = Ae^{-x^2+2ix} \quad (28)$$

where the constant A denotes the height of the initial pulse. This initial pulse propagates along the x -axis as time proceeds. The choice $A = 1$ causes the initial pulse of unit height to fade out depending on the proceeding time, Fig 8(a). The designed routines are run up to the time $t = 6$ with a fixed $\Delta x = 0.25$ and $\kappa = 2$ over the problem interval $[-30, 60]$ to simulate the solutions illustrating the birth of propagating pulse for $A = 1.78$, Fig 8(b). This choice of A produces an initial pulse of height 1.78. The height increases over 2 and two bulges begin to appear at both sides of the pulse at the earlier times of the solution. These two bulges moves far away from the pulse. Subsequently, the height comes below 2 and stays fixed around 1.9. The two bulges moving far away from the pulse lose their heights but widen as time goes.

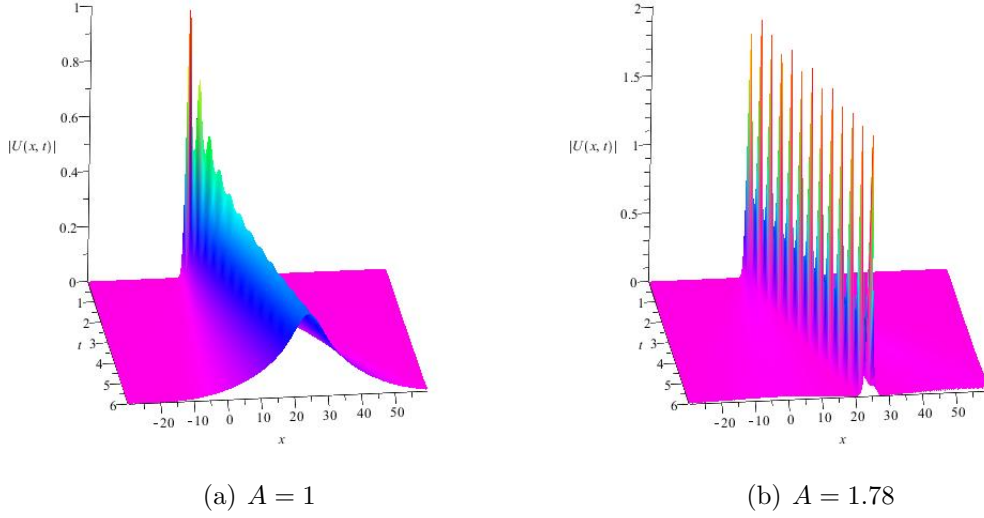


Figure 8: The behaviors of the propagating pulse depending on A

The conservation laws are calculated initially as $C_1 = 3.971000512$ and $C_3 = 10.95838443$. The second order methods HEUN and RK2 fail to give the solutions when $\Delta t = 0.01$ owing to the instability, Table 4. The reduction of Δt to 0.001 resolve this issue by giving six decimal-digit preservation in the C_1 and four decimal-digit preservation in the C_3 at the simulation ending time $t = 6$ for both methods. The RK3 generates three decimal-digit preservation in both of the conservation laws with the discretization parameters $\Delta x = 0.25$ and $\Delta t = 0.01$. When the time step size is reduced to 0.001, the preservation of the absolute relative changes of both C_1 and C_3 improve to six and four decimal digits, respectively. $\Delta t = 0.01$ gives five, six and seven decimal-digit preservation in the values of C_1 for the methods RK4, RK5 and CK, again respectively. This choice of Δt preserves the C_3 in four decimal digits for all the higher order methods RK4, RKF and CK. Even though decreasing the time step size to 0.001 improve the preservation in C_1 more than ten decimal digits, no decimal digit improvement in the preservation is observed in the value of the C_3 .

The eigenvalue distributions of coefficient matrices are graphed in Fig 9(a) - 9(b). The maximum complex component in absolute value of all eigenvalues is 157.267 requires smaller Δt values in the lower order methods HEUN and RK2. $\lambda_j \times \Delta t$ is not sufficient to satisfy the stability condition given in Fig 1(a) when $\Delta t = 0.01$. The choices of time step size for the other methods used in this study supply with the stability condition.

Table 4: Absolute relative changes of the conservation laws at $t = 6$ for the birth of propagating pulse

Method	Δx	Δt	$C(C_1(6))$	$C(C_3(6))$
HEUN (present)	0.25	0.01	∞	∞
HEUN (present)	0.25	0.001	4.474×10^{-6}	1.835×10^{-4}
RK2 (present)	0.25	0.01	∞	∞
RK2 (present)	0.25	0.001	4.474×10^{-6}	1.835×10^{-4}
RK3 (present)	0.25	0.01	1.314×10^{-3}	4.865×10^{-3}
RK3 (present)	0.25	0.001	1.491×10^{-6}	2.113×10^{-4}
RK4 (present)	0.25	0.01	1.462×10^{-5}	3.862×10^{-4}
RK4 (present)	0.25	0.001	$< 10^{-10}$	2.041×10^{-4}
RKF (present)	0.25	0.01	1.779×10^{-6}	1.816×10^{-4}
RKF (present)	0.25	0.001	$< 10^{-10}$	2.041×10^{-4}
CK (present)	0.25	0.01	2.727×10^{-7}	1.995×10^{-4}
CK (present)	0.25	0.001	$< 10^{-10}$	2.041×10^{-4}
CDQ [27]	0.25	0.01	1.461×10^{-5}	1.824×10^{-4}
PDQ [28]	0.25	0.01	1.575×10^{-5}	5.265×10^{-4}

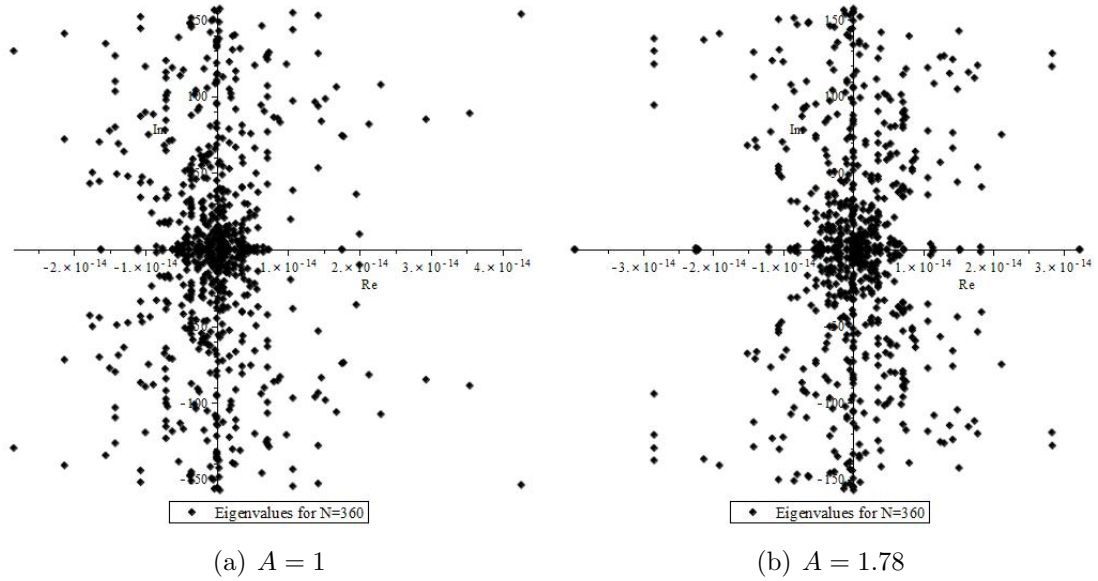


Figure 9: The behaviors of the propagating pulse depending on A

5.5 Bound State of n solitons

The bound state of n solitons for the nonlinear cubic NLS equation (1) is simulated with the initial data

$$u(x, 0) = \text{sech } x \quad (29)$$

where $\kappa \geq 2n^2$, $n \in \mathbb{Z}^+$ in the NLS equation (1) [1, 13]. When this condition on κ is satisfied, the $u(x, t)$ gives n -soliton bound state type solution and the periodicity property in a mobile frame of the solution is fulfilled. The case $2n^2 < \kappa < 2(n+1)^2$ causes the asymptotic solution to include both bound state and an oscillation with $O(t^{-1/2})$ as $\kappa < 2$ gives only the oscillation [13]. Unfortunately, the larger values of n is not sufficiently suitable for the numerical solutions. In the present study, the behaviors are investigated for $n = 2, 3, 4$ in the interval $[-20, 20]$. The designed algorithms are run by using the discretization parameters $\Delta x = 0.125$ and $\Delta t = 0.001$ up to the ending time $t = 0.6$.

In the first experiment, n is chosen as 2. The initial data stands for a pulse of unit height positioned at $x = 0$, Fig 10(a). When the time reaches $t = 0.2$ the height of the pulse passes over 1.2, Fig 10(b). Two bulges begin to appear at both sides of this pulse when the time is $t = 0.3$, Fig 10(c), as the peak gets higher than 1.6. These two bulges are separated from the pulse at the time $t = 0.4$, Fig 10(d). As the time proceeds, the bulges merges to the pulse again at $t = 0.5$, Fig 10(e). However, the height of the pulse descends down 1.6. At the end of the simulation, the height is measured just over 1.2 and the bulges disappear, Fig 10(f).

The choice of $n = 3$ is studied in the same interval up to the ending time $t = 0.6$ using the same discretization parameters. The initial pulse of height 1 gives birth two new bulges at both sides as the simulation time reaches $t = 0.175$ and its height passes over 2, Fig 11(a). These two bulges join back to the pulse but then the pulse begins to split in two halves vertically starting in the peak as time proceeds to $t = 0.250$, Fig 11(b). Following the split of the pulse, two bulges begin to appear at the sides of these two halves of the pulse at $t = 0.300$, Fig 11(c), and become evident at $t = 0.325$, Fig 11(d). As time proceeds to 0.400 and 0.500, the two halves of the pulse and the bulges join together back and become a unique pulse of height over 1.8, Fig 11(e) - Fig 11(f). The similar behaviors keep at the remaining time of the simulation.

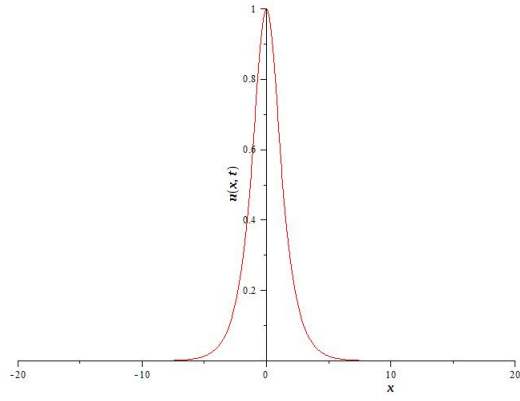
When $n = 4$, the initial pulse of unit height splits in two high pulses of heights over 1.6 with one bulge at the other sides of each at $t = 0.175$, Fig 12(a). As time proceeds the number of bulges increases at both sides of twin longer pulses at time $t = 0.225$, Fig 12(b). At $t = 0.375$, two well shaped pulses and a longer pulse of height over 1.6 between them are observed clearly, Fig 12(c). There are three smaller bulges at both sides of these three pulses at this time. The twin pulses and the longer pulse positioned between them separate clearly from each other at $t = 0.475$, Fig 12(d). The other smaller pulses propagate along the horizontal axis

and get far away from these three longer pulses. The twins and the longer pulse joins together again at $t = 0.550$, Fig 12(e). The heights of the twins approaches 1 as the longer one gets shorter at this time. When the time is 0.600, the twin pulses gets smaller in height as the longer one gets higher, Fig 12(f).

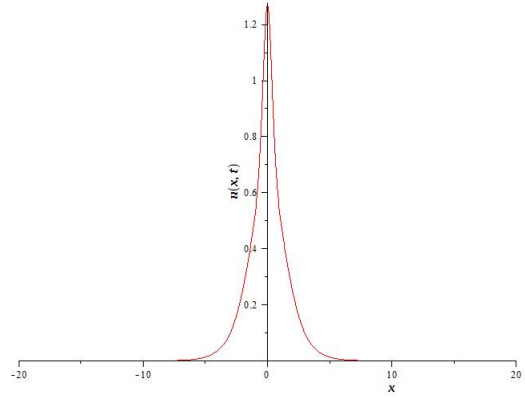
In conclusion, when the number n increases, the formation of new solitons are more rapidly and the number of those solitons increases. The solitons do not exceed the imaginary bounds while they are forming and disappearing during the simulations. This status corresponds to the theoretical aspects and the earlier findings reported in the numerical studies.

The absolute relative changes of the conservation laws for the experiments obtained for various values of n are illustrated in Table 5. The initial values of the conservation laws are determined as $C_1 = 2$ and $C_3 = (2/3)(1 - \kappa)$. Both conservation laws remain almost constant for all cases and the absolute relative changes are the indicators of satisfactory as tabulated in the table.

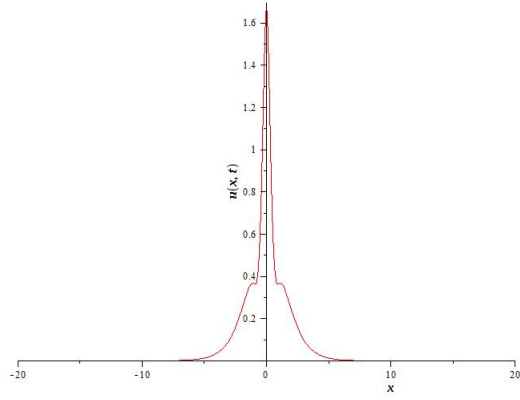
The eigenvalue distributions of all cases $\kappa = 2, 3, 4$ are depicted in Fig 13(a)-13(c). The maximum and minimum complex components of all eigenvalues are determined as ± 628.749 for all choices of κ . $\Delta t = 0.001$ is sufficient to provide the stability for all methods used to solve the bound state of solitons problem.



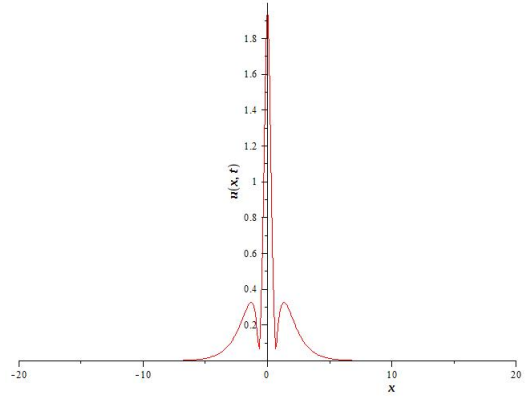
(a) $t = 0$



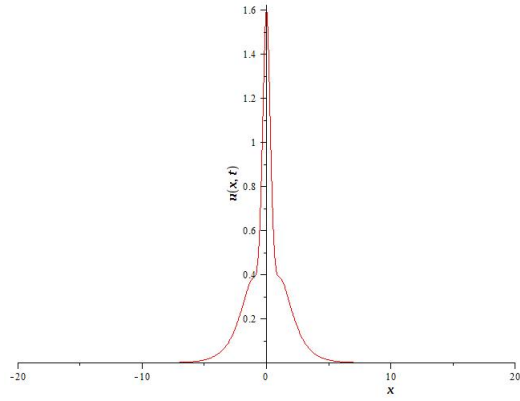
(b) $t = 0.2$



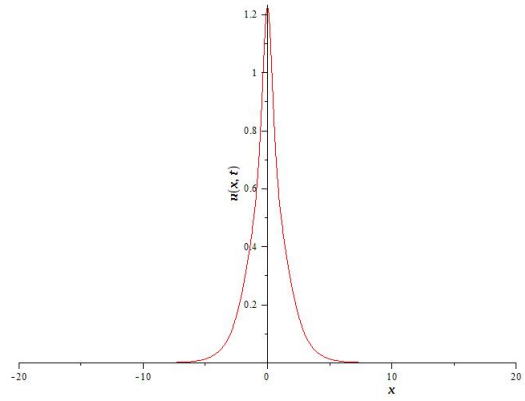
(c) $t = 0.3$



(d) $t = 0.4$

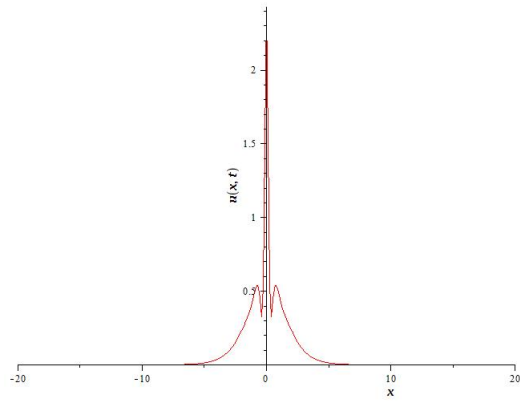


(e) $t = 0.5$

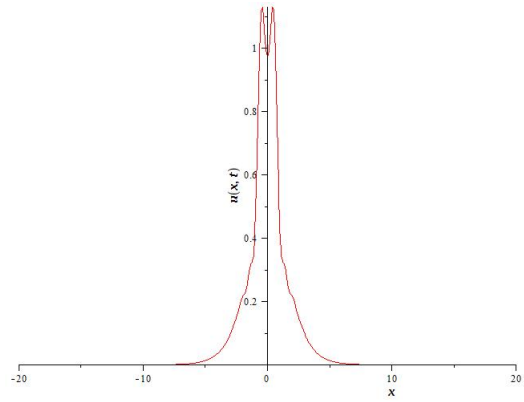


(f) $t = 0.6$

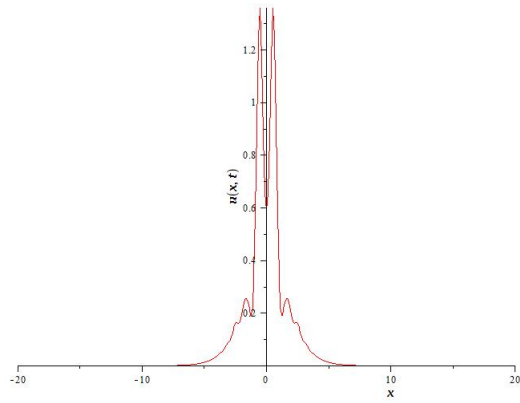
Figure 10: Bound state of solitons for $n = 2$



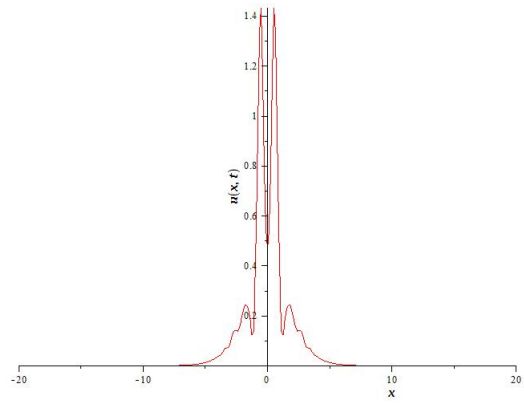
(a) $t = 0.175$



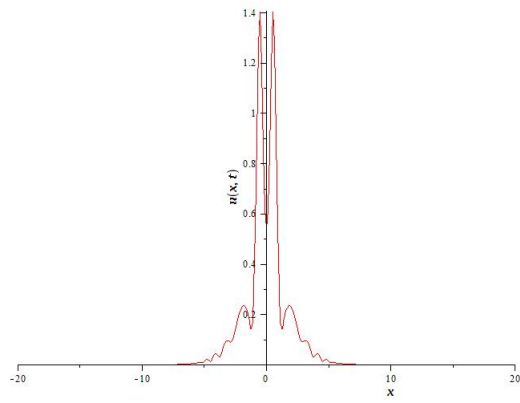
(b) $t = 0.250$



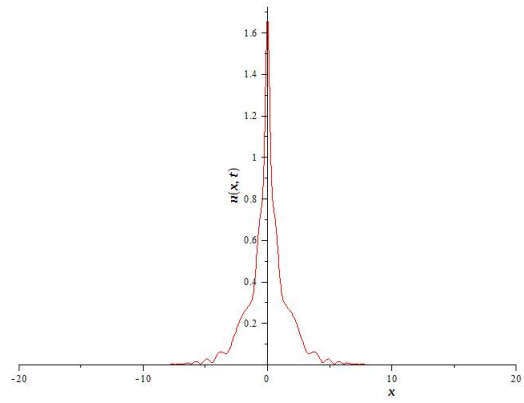
(c) $t = 0.300$



(d) $t = 0.325$

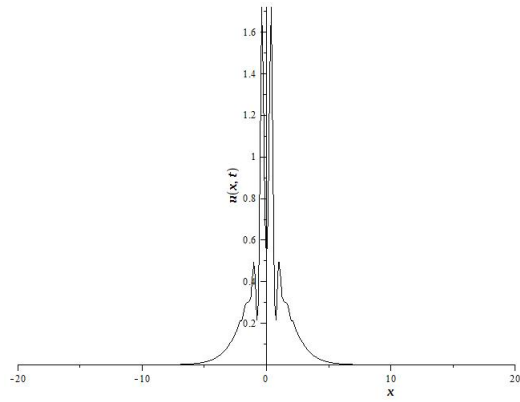


(e) $t = 0.400$

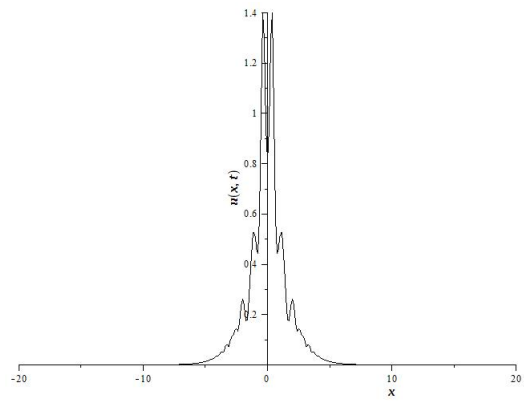


(f) $t = 0.500$

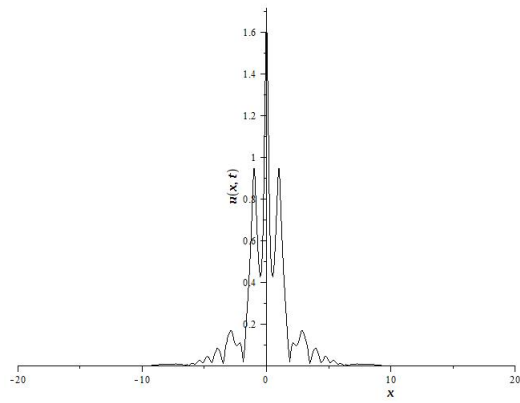
Figure 11: Bound state of solitons for $n = 3$



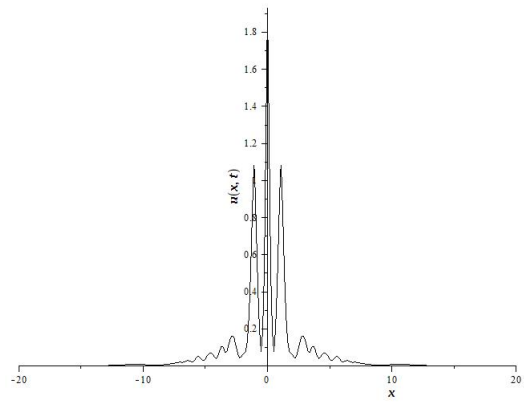
(a) $t = 0.175$



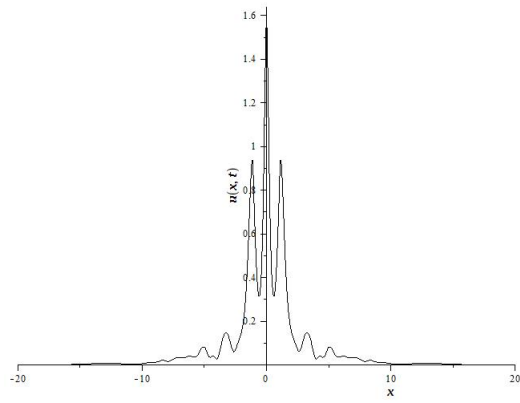
(b) $t = 0.225$



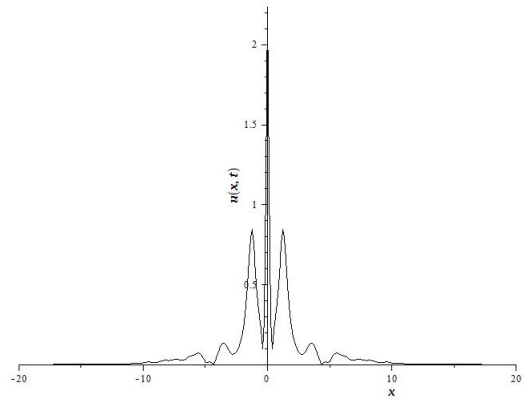
(c) $t = 0.375$



(d) $t = 0.475$



(e) $t = 0.550$



(f) $t = 0.600$

Figure 12: Bound state of solitons for $n = 4$

Table 5: Absolute relative changes of the conservation laws at $t = 0.6$ for the birth of propagating pulse

Method	Δx	Δt	n	$C_1(0)$	$C_3(0)$	$C(C_1(0.6))$	$C(C_3(6))$
HEUN	0.125	0.001	2	2	-4.666666666	1.964×10^{-6}	1.312×10^{-6}
RK2						1.964×10^{-6}	1.311×10^{-6}
RK3						6.540×10^{-7}	4.586×10^{-6}
RK4						$< 10^{-10}$	6.428×10^{-10}
RKF						5.000×10^{-10}	8.571×10^{-10}
CK						5.000×10^{-10}	8.571×10^{-10}
HEUN			3	2	-11.33333333	1.767×10^{-4}	1.365×10^{-3}
RK2						1.767×10^{-4}	1.365×10^{-3}
RK3						5.629×10^{-5}	6.353×10^{-4}
RK4						3.400×10^{-8}	7.292×10^{-6}
RKF						7.500×10^{-9}	7.238×10^{-6}
CK						7.000×10^{-9}	7.314×10^{-6}
HEUN			4	2	-20.66666666	5.095×10^{-3}	6.238×10^{-2}
RK2						5.095×10^{-3}	6.238×10^{-2}
RK3						7.151×10^{-4}	8.245×10^{-3}
RK4						1.587×10^{-6}	6.432×10^{-4}
RKF						5.142×10^{-8}	6.481×10^{-4}
CK						7.675×10^{-7}	6.370×10^{-4}
CDQ [27]	0.125	0.0025	3			3.282×10^{-6}	5.201×10^{-4}
CDQ [27]	0.125	0.0025	4			1.922×10^{-4}	1.558×10^{-3}
PDQ [28]	0.1	0.01	4			1.174×10^{-7}	5.127×10^{-5}

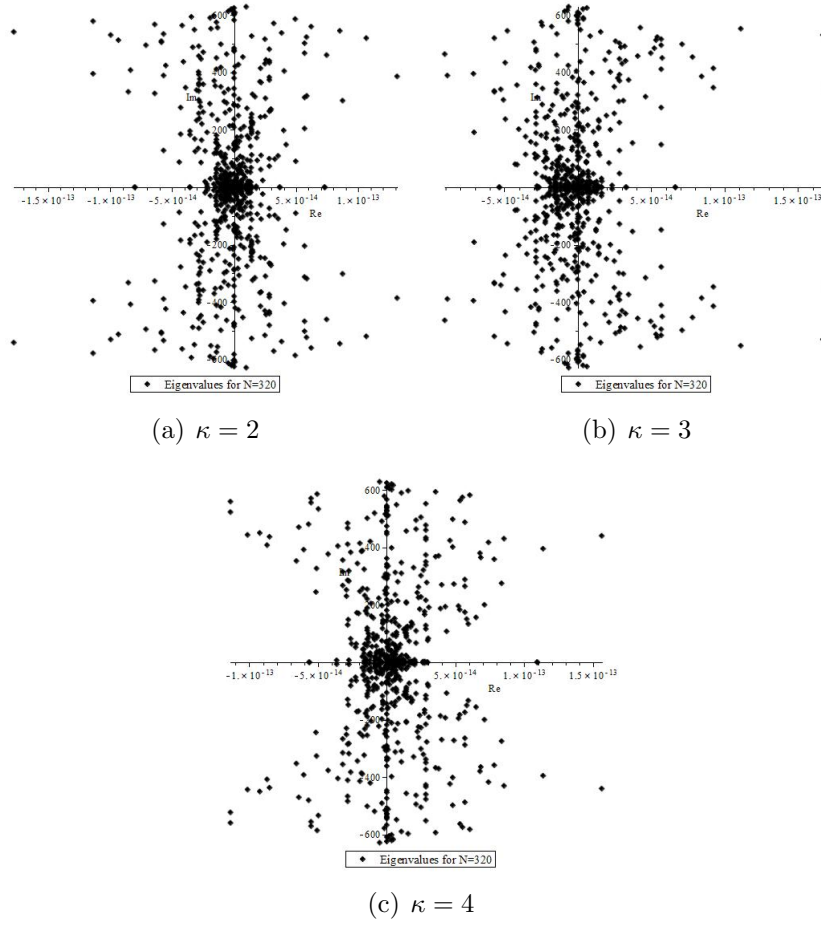


Figure 13: The eigenvalue distribution for bound state of solitons

6 Conclusion

Some dynamic problems constructed on the nonlinear cubic NLS equation are solved by differential quadrature method based on sine cardinal functions. The dimension reduced form of the equation is integrated using various methods of different orders. The absolute relative changes are computed in each case to validate the accuracy of the method even analytical solutions do not exist.

The discretization parameter Δt is successfully selected to satisfy the stability condition. The instability of some lower order methods, particularly, explained by coinciding the theoretical aspects and matrix stability analysis via eigenvalues for all experiments.

The comparison with earlier studies covering some differential quadrature techniques indicate that the proposed algorithms also generate acceptable results. In

many cases, the results seem more accurate even when less grids are used. When compared with the collocation or finite element methods, the programming is easier owing to the main logic that approximates directly to the derivative. Particularly, it also enables using higher order time integration techniques more easily. On the other hand, memory allocation and number of algebraic calculations can be discussed when compared the other method families.

7 Acknowledgment

This study (Research Project Number BAP-FF160316B19) is supported by The Scientific Research Projects Unit at Çankırı Karatekin University, Turkey.

References

- [1] V.E. Zakharov, A. B. Shabat, Exact Theory of two-dimensional self-focusing and one-dimensional self-modulation of waves in nonlinear media, Soviet Physics JETP, 34, 1, 62-69 1972.
- [2] V. I. Talanov, Self-focusing of wave beams in nonlinear media, JETP Lett. 2, 138-141, 1965.
- [3] V. I. Bespalov, A. G. Litvak, and V.I. Talanov, II Vsesoyuznyi simpozium po nelineinoi optike (Second All-union Symposium on Nonlinear Optics), 1966, Collection of Papers, Nauka, 1968.
- [4] V. E. Zakharov, Dissertation, Institute of Nuclear Physics, Siberian Division, USSR Academy of Sciences, 1966.
- [5] Peregrine, D. H. (1983). Water waves, nonlinear Schrödinger equations and their solutions. The Journal of the Australian Mathematical Society. Series B. Applied Mathematics, 25(01), 16-43.
- [6] Debnath, L., Nonlinear Partial Differential Equations for Scientists and Engineers, Birkhauser Springer Science, Boston, 2005.
- [7] Yajima, N., & Outi, A. (1971). A new example of stable solitary waves. Progress of theoretical physics, 45(6), 1997-1998.
- [8] Ablowitz, M. J., & Segur, H. (1979). On the evolution of packets of water waves. Journal of Fluid Mechanics, 92(04), 691-715.

- [9] Thyagaraja, A. (1981). Recurrence, dimensionality, and Lagrange stability of solutions of the nonlinear Schrödinger equation. *Physics of Fluids* (1958-1988), 24(11), 1973-1975.
- [10] Pitaevskii, L. P. (1961). Vortex lines in an imperfect Bose gas. *Sov. Phys. JETP*, 13, 451-454.
- [11] Whitham, G.B., *Linear and Nonlinear Waves*, John Wiley & Sons, Inc., New York, 1999.
- [12] Tsuzuki, T. (1971). Nonlinear waves in the Pitaevskii-Gross equation. *Journal of Low Temperature Physics*, 4(4), 441-457.
- [13] Miles, J. W. (1981). An envelope soliton problem. *SIAM Journal on Applied Mathematics*, 41(2), 227-230.
- [14] Bu, C. (1996). Generalized solutions to the cubic Schrödinger equation. *Non-linear Analysis: Theory, Methods & Applications*, 27(7), 769-774.
- [15] Zakharov, V. E., & Shabat, A. B. (1973). Interaction between solitons in a stable medium. *Soviet Journal of Experimental and Theoretical Physics*, 37, 823.
- [16] Öziş, T., & Yıldırım, A. (2008). Reliable analysis for obtaining exact soliton solutions of nonlinear Schrödinger (NLS) equation. *Chaos, Solitons & Fractals*, 38(1), 209-212.
- [17] Khuri, S. A. (2004). A complex tanh-function method applied to nonlinear equations of Schrödinger type. *Chaos, Solitons & Fractals*, 20(5), 1037-1040.
- [18] Taha, T. R. (1991). A numerical scheme for the nonlinear Schrödinger equation. *Computers & Mathematics with Applications*, 22(9), 77-84.
- [19] Dereli, Y., Irk, D., & Dag, I. (2009). Soliton solutions for NLS equation using radial basis functions. *Chaos, Solitons & Fractals*, 42(2), 1227-1233.
- [20] Chang, Q., Jia, E., & Sun, W. (1999). Difference schemes for solving the generalized nonlinear Schrödinger equation. *Journal of Computational Physics*, 148(2), 397-415.
- [21] Dag, I. (1999). A quadratic B-spline finite element method for solving nonlinear Schrödinger equation. *Computer methods in applied mechanics and engineering*, 174(1-2), 247-258.

- [22] Gardner, L. R. T., Gardner, G. A., Zaki, S. I., & El Sahrawi, Z. (1993). B-spline finite element studies of the non-linear Schrödinger equation. *Computer methods in applied mechanics and engineering*, 108(3), 303-318.
- [23] Aksoy, A. M., Irk, D., & Dag, I. (2012). Taylor collocation method for the numerical solution of the nonlinear Schrödinger equation using quintic B-spline basis. *Physics of Wave Phenomena*, 20(1), 67-79.
- [24] Robinson, M. P., Fairweather, G., & Herbst, B. M. (1993). On the numerical solution of the cubic Schrödinger equation in one space variable. *Journal of Computational Physics*, 104(1), 277-284.
- [25] Twizell, E. H., Bratsos, A. G., & Newby, J. C. (1997). A finite-difference method for solving the cubic Schrödinger equation. *Mathematics and computers in simulation*, 43(1), 67-75.
- [26] Cenicerros, H. D. (2002). A semi-implicit moving mesh method for the focusing nonlinear Schrödinger equation. *Commun. Pure Appl. Anal*, 1(1), 1-18.
- [27] Korkmaz, A., & Dag, I. (2008). A differential quadrature algorithm for simulations of nonlinear Schrödinger equation. *Computers & Mathematics with Applications*, 56(9), 2222-2234.
- [28] Korkmaz, A., & Dag, I. (2009). A differential quadrature algorithm for nonlinear Schrödinger equation. *Nonlinear Dynamics*, 56(1-2), 69-83.
- [29] Bellman, R., Kashef, B. G., & Casti, J. (1972). Differential quadrature: a technique for the rapid solution of nonlinear partial differential equations. *Journal of computational physics*, 10(1), 40-52.
- [30] Bashan, A., Karakoc, S. B. G., & Geyikli, T. (2015). Approximation of the KdVB equation by the quintic B-spline differential quadrature method. *Kuwait Journal of Science*, 42(2).
- [31] Korkmaz, A. (2010). Numerical algorithms for solutions of Korteweg-de Vries equation. *Numerical methods for partial differential equations*, 26(6), 1504-1521.
- [32] Arora, G., & Singh, B. K. (2013). Numerical solution of Burgers' equation with modified cubic B-spline differential quadrature method. *Applied Mathematics and Computation*, 224, 166-177.

- [33] Mittal, R. C., & Jiwari, R. (2011). Numerical study of two-dimensional reaction-diffusion Brusselator system by differential quadrature method. *International Journal for Computational Methods in Engineering Science and Mechanics*, 12(1), 14-25.
- [34] Tamsir, M., Srivastava, V. K., & Mishra, P. D. (2016). Numerical simulation of three dimensional advection-diffusion equations by using modified cubic B-spline differential quadrature method. *Asia Pacific Journal of Engineering Science and Technology*, 2(7), 1-13.
- [35] F. Stenger, *Numerical Methods Based on Sinc and Analytic Functions*, Springer, New York, 1993.
- [36] T. S. Carlson, J. Dockery, J. Lund, A sinc-collocation method for initial boundary value problems, *Mathematics of Computation* 66 (1997) 215–235.
- [37] A. Secer, Numerical solution and simulation of second-order parabolic pdes with sinc-galerkin method using maple, *Abstract and Applied Mathematics* Article ID 686483 (2013) 1–10.
- [38] M. Dehghan, A. Saadatmandi, The numerical solution of a nonlinear system of second-order boundary value problems using the sinc-collocation method, *Mathematical and Computer Modelling* 46 (2007) 1434-1441.
- [39] J. Lund, K. L. Bowers, *Sinc Methods for Quadrature and Differential Equations*, SIAM, Philadelphia, 1992.
- [40] Bellomo, N., & Ridolfi, L. (1995). Solution of nonlinear initial-boundary value problems by sinc collocation-interpolation methods. *Computers & Mathematics with Applications*, 29(4), 15-28.
- [41] A. Korkmaz, I. Dağ, Shock wave simulations using sinc differential quadrature method, *Engineering Computations* 28 (2011) 654-674.